
LEVERAGING IMAGE-BASED GENERATIVE ADVERSARIAL NETWORKS FOR TIME SERIES GENERATION

A PREPRINT

Justin Hellermann
Stefan Lessmann

Humboldt University of Berlin
 School of Business and Economics
 Unter den Linden 6
 10099 Berlin
 {justin.hellermann, stefan.lessmann}@hu-berlin.de

December 16, 2021

ABSTRACT

Generative models synthesize image data with great success regarding sampling quality, diversity and feature disentanglement. Generative models for time series lack these benefits due to a missing representation, which captures temporal dynamics and allows inversion for sampling. The paper proposes the intertemporal return plot (IRP) representation to facilitate the use of image-based generative adversarial networks for time series generation. The representation proves effective in capturing time series characteristics and, compared to alternative representations, benefits from invertibility and scale-invariance. Empirical benchmarks confirm these features and demonstrate that the IRP enables an off-the-shelf Wasserstein GAN with gradient penalty to sample realistic time series, which outperform a specialized RNN-based GAN, while simultaneously reducing model complexity.

Keywords Intertemporal Return Plot · IRP · Generative Adversarial Networks · Time Series · Recurrence Plots

1 Introduction

Generative adversarial networks (GANs) are a state-of-the-art approach to synthesize data in several domains and applications. Recent advances cover artificial medical data (Shin et al., 2018), encryption (Sirichotendumrong and Kiya, 2020) as well as image segmentation (Isola et al., 2018). Especially the work of Karras et al. (2019) received wide recognition due to the ability to synthesize almost indistinguishable fake images of faces with disentangled, controllable features.

While the synthesis of images is a relatively young field, the simulation of time series and especially price paths originated decades ago. Early approaches use parametric models, which requires knowledge about the underlying dynamics or strict assumptions on the process. This may be appropriate for some controllable processes but becomes a bottleneck once dimensionality increases or non-stationarity is present. Then, parametric models need continuous recalibration to sustain their effectiveness. To remedy this, nonparametric models are increasingly used for generating time series data. Contrary to the CNN-based models used for image data generation, RNN-based time series GAN models are often complex and consist of numerous networks, encoding/decoding steps, and loss functions. Inspired by recent successes in computer vision, multiple attempts have been made to simulate time series using convolutional neural networks (Brophy et al., 2019; Smith and Smith, 2021). However, these approaches lack a proper image representation of the time series. More specifically, no existing representation provides all of the following desiderata: i) the ability to capture temporal dynamics, ii) invertibility of the representation for generating new time series, and iii) invariance to the scale of features.

The paper proposes the intertemporal return plot (IRP), a new image representation for time series. The IRP facilitates

synthesizing time series using generative image models. This way, time series generation can immediately benefit from the latest advances in computer vision while avoiding the need for specialized and complex generative models for time series. The IRP is promising approach to benefit from these advances and to improve time series data augmentation models, which can be used to either complement missing data, avoid high costs of data collection as well as to improve robustness and backtests of forecasting models. The new approach compensates the limitations of existing representations by capturing the underlying dynamics of a time series and providing an invertible, scale-invariant approach to recover the time series from the image representation without adding extra model complexity. Empirical tests confirm the effectiveness of the IRP and show image-based generative models trained based on our IRP to yield higher sample quality than state-of-the-art time series GANs.

2 Related Work

The challenge of generating of time series stems from changes in the intertemporal dynamics, the presence of jumps, and correlations between multiple time series. The prevailing approaches rely on recurrent neural networks (Yoon et al., 2019) (Koochali et al., 2019) and address these challenges by adding complexity. The most prominent RNN-based model is the TimeGAN of Yoon et al. (2019). To outperform other RNN-based models, TimeGAN balances five different loss function that control the generator, the discriminator, intertemporal relationships, moments, and the embedding loss. The TimeGAN architecture assigns each network a different task and each component is trained separately before starting a joint training. Distributing TimeGAN computations is complicated, which leads to long training procedures.

Other approaches use convolutional neural networks to simulate image representations of time series (Donahue et al., 2019) (Smith and Smith, 2021) and are currently dominated by the use of spectrograms and waveforms. Spectrograms process audio signals and visualize the spectrum of frequencies of a signal as it varies with time (Wyse, 2017) while each plot is characteristic for a certain sound or a spoken word. In a recent paper, Smith and Smith (2021) propose a GAN model with a simplified, image-based approach using two separate Wasserstein GANs. The first network takes the spectral image of the signal and generates new spectrograms. Thereafter, the other GAN generates a candidate signal that is likely to have created that spectrogram. Both GAN finally unify their loss functions in a joint expression in order to facilitate training. The reason for using two GAN is that since the initial time series cannot be inverted in a deterministic way, the second GAN is needed to construct an estimate. Due to the spectrogram representation and its non-invertibility, the sampling process requires increased complexity. Thus, the two GAN approach is a drawback. A second image representation of a time series is a waveform. It can be processed by CNNs and refers to the shape of its graph as a function of time and is used by Donahue et al. (2019) to simulate new time series. The advantage is that the representation works well for image generation while capturing the non-stationary components of a time series. The ability of waveforms to capture non-stationary data has been extensively studied in, for example, electric engineering (Wyse, 2017) (Afroni et al., 2013). However, the inversion appears difficult, as pointed out by Donahue et al. (2019). They demonstrate that even if inversion is approximately possible via the Griffin-Lim algorithm, the sample quality is not significantly better than using an additional inference network.

As a result, image-based methods currently lack an efficient representation that captures the dynamics of a time series while being invertible. The new method proposed in this paper solves both problems.

3 Methodology

This section briefly reviews existing image representations of time series before introducing the proposed IRP approach. Thereafter, we revisit the Wasserstein GAN with gradient penalty, which is used in the empirical part of the paper. A first approach towards a meaningful time series image representation was developed in the 1980's by Eckmann et al. (1987). It has found frequent application, especially in chaos theory (Marwan et al., 2007) and system engineering (Curry, 2012), to identify the state of an underlying system. To achieve this, the authors introduce the recurrence plot that depicts points in which the time series has approximately the same value. All recurrences of a time series are obtained by calculating

$$R_{i,j}^B = \begin{cases} 1 & \text{if } \|x_i - x_j\| \leq \varepsilon \\ 0 & \text{otherwise,} \end{cases} \quad \forall i, j \in \{1, 2, \dots, S\} \quad (1)$$

with $R_{i,j}^B$ being an $S \times S$ matrix with indexes i and j . The representation has some similarity with a (binary) correlation matrix where each step in time corresponds to a feature and S corresponds to the sequence length. A recurrence is present, if the absolute difference between the values at time i and j is smaller than a threshold ε . By definition, the diagonal d of $R_{i,j}^B$ is filled with recurrences $\forall i, j \in \{1, 2, \dots, S\}, i = j \implies d_{i,j} = 1$. Consideration of the absolute difference also implies symmetry, $R_{i,j}^B = R_{j,i}^B$.

Recurrence plots can reveal characteristics like trends, jumps, and cyclic behavior and incorporate major statistical properties. To extract these characteristics, recurrence plot quantification analysis (RQA) offers several proxies for the predictability of the underlying process or how long it remains in a certain state (Marwan et al., 2007).

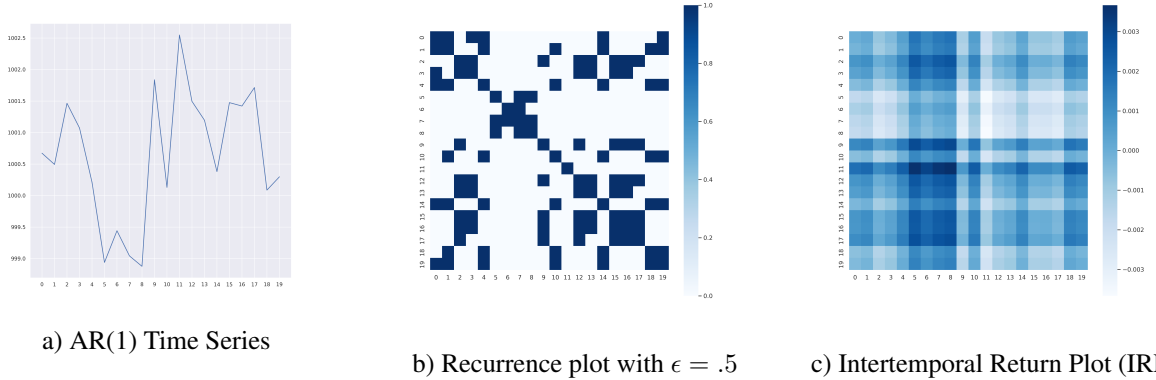
Recurrence plots are powerful for time series analysis but require adjustments to serve as image representation for sampling new time series. The adjustment is needed because a recurrence only states whether a time series has come significantly close to a previous value. Since "non-recurrences" can hypothetically take any value, they provide no information for the generating process and make a binary recurrence plot irreversible.

To achieve reversibility of a time series, instead of evaluating whether an absolute difference of times series values at index i and j exceeds ϵ , we can either use the difference between both values or their ratio. Differencing a time series stabilizes it in terms of the mean and mitigates the impact of trend and seasonality (Sutcliffe, 1994). Thus, it is a measure to transform a time series towards stationarity. This concept is popular in economics and quantitative finance and has shown to work well in many applications (Hudson and Gregoriou, 2010).

Another approach involves calculating logarithmic returns, or log returns. The log transformation has a similar effect on the time series as differencing. However, calculating returns has the advantage of being invariant to scale and is especially useful when the time series evolves. Further, log returns have the desirable statistical characteristic of approximate normality (Wilmott, 2006, p. 295). Thus, we use log returns and create what we call the *intertemporal return plot* $R_{i,j}^C$ as:

$$R_{i,j}^C = \log \left(\frac{x_i}{x_j} \right) \quad \forall i, j \in \{1, 2, \dots, S\} \quad (2)$$

Once the start value at $t = 0$ is known, the initial trajectory can be recovered from the IRP regardless of whether it is a real or simulated representation. An additional advantage of the IRP over the binary recurrence plot is the absence of ϵ , the correct specification of which is complicated and may change over time. Figure 1 displays an AR1 process and



a) AR(1) Time Series b) Recurrence plot with $\epsilon = .5$ c) Intertemporal Return Plot (IRP)

Figure 1: AR time series with binary and intertemporal return plot

compares the binary representation of the recurrence plot to the proposed IRP representation. Similar structures can be found in both plots, while the IRP provides a more granular version of the binary recurrence plot. Following this visual inspection, we next discuss generative models for creating synthetic IRPs.

In computer vision, GANs are a state-of-the-art model class for generating image data. The idea of a GAN is to train a generator network G and a discriminator network D with opposing objective functions. In the course of training, G generates a fake distribution \tilde{x} and proposes it to D . Next, D assesses the likelihood of \tilde{x} originating from the true data distribution. The adversarial game between G and D can be described by the objective function

$$\min_G \max_D \mathbb{E}_{x \sim \mathbb{P}_r} [\log(D(x))] + \mathbb{E}_{\tilde{x} \sim \mathbb{P}_g} [\log(1 - D(\tilde{x}))] \quad (3)$$

where the discriminator and generator try to maximize and minimize (3), respectively. $D(x)$ is the estimate of the discriminator that x is real while \mathbb{P}_r denotes the real data distribution. The generated data is denoted by \tilde{x} with $\tilde{x} = G(z)$ and $z \sim p(z)$ where p denotes some distribution, such as uniform or Gaussian. \mathbb{P}_g is the distribution of the generated data, or, put differently, the model distribution. Having the opposing objectives, both networks play an iterative game and train each other in the process.

The above vanilla GAN suffers from stability problems and is difficult to train (Goodfellow et al., 2014). Arjovsky et al. (2017) address this problem by proposing a Wasserstein-GAN (WGAN). WGAN shows a more stable training behavior as well as correlation between the value of the objective function and sample quality. An intuitive explanation for the

Wasserstein distance as a loss function can be obtained from its synonym *Earth Mover Distance*. It can be related to the minimum cost of transporting mass in order to transform the distribution q into the distribution p , whereby the cost is mass times transport distance. The Wasserstein metric changes the upper objective function to

$$\min_G \max_{D \in \mathcal{D}} \mathbb{E}_{x \sim \mathbb{P}_r} [D(x)] - \mathbb{E}_{\tilde{x} \sim \mathbb{P}_g} [D(\tilde{x})] \quad (4)$$

where \mathcal{D} is defined as a set of 1-Lipschitz functions and \tilde{x} is a randomly sampled subset. Instead of classifying generated images as real or fake, the WGAN replaces the discriminator model by a critic that scores the realness or fakeness of an image. Gulrajani et al. (2017) further improve training in their WGAN-GP, which incorporates gradient penalty terms for the discriminative network. This changes the objective function to

$$\min_G \max_{D \in \mathcal{D}} \mathbb{E}_{x \sim \mathbb{P}_r} [D(x)] - \mathbb{E}_{\tilde{x} \sim \mathbb{P}_g} [D(\tilde{x})] + \lambda \mathbb{E}_{\tilde{x} \sim \mathbb{P}_{\hat{x}}} [(\|\nabla_{\tilde{x}} D(\tilde{x})\|_2 - 1)^2] \quad (5)$$

The gradient penalty term $[(\|\nabla_{\tilde{x}} D(\tilde{x})\|_2 - 1)^2]$ opposes vanishing and exploding gradients. We refer to Gulrajani et al. (2017) for a more detailed explanation of all underlying concepts and considerations.

4 Experiments

Section 1 introduces the desiderata of an image representation for time series. Since the IRP is scale-invariant and invertible by design, the key question to answer by empirical experimentation is whether the IRP captures temporal dynamics. To test this, we conduct a series of experiments starting with a qualitative visual inspection of simulation results by a WGAN-GP trained on IRP representations. We consider time series with different characteristics to ensure the generation process generalizes well.

For the visual inspection, the first step is to calculate the IRPs for a set of real time series. In a next step, the WGAN-GP model is trained to simulate synthetic IRPs. Afterwards, the invertability of the IRP facilitates obtaining a synthetic time series given some start value c . Last, we cluster synthetic and original time series to facilitate visual comparisons. Each real and generated time series is represented by a single dot in a two-dimensional space. Elements that are close in the two-dimensional space are likely to have similar characteristics in the higher dimensional space. The method used for clustering is the Uniform Manifold Approximation and Projection (UMAP) algorithm (McInnes et al., 2020), which interprets each of the d time steps as an individual feature. A similar approach for clustering time series has been applied by Yoon et al. (2019); Ali et al. (2019). In case real and synthetic elements are different, the UMAP algorithm forms separate, homogeneously colored clusters with little distance between the elements inside each cluster and large distances between the individual clusters. Coloring the elements in the plot visualizes their class membership of either real (green) or synthetic (red). In case the real and synthetic time series are similar, the algorithm returns heterogeneous clusters of mixed red and green dots.

The series of qualitative experiments starts with an autoregressive process defined by $X_t = c + \sum_{i=1}^p \varphi_i X_{t-i} + \varepsilon_t$ with $\varphi = 0.9$ and $p = 1$. We simulated $N = 1000$ time series with length $S = 28$ and $c = 100$. In a following step, the WGAN-GP synthesized the IRPs of the AR process and we generate the synthetic time series from the IRPs. Figure 2a) reveals that the UMAP algorithm forms four separate clusters. However, each cluster is heterogeneous in the sense that it comprises real and synthetic time series. The inability of the UMAP algorithm to separate the two types of time series evidences that the synthetic time series are realistic. Figure 2b) contains the images of four synthetic IRPs with $S = 28$ and the corresponding recovered time series starting from $c = 100$. Neither the synthetic IRPs nor the time series show any obvious irregularities. Further, recall that the upper triangular of an IRP is, by definition, equal to the inverted lower triangular. A visual inspection of Figure 2b) suggests that the synthetic IRPs exhibit this characteristic. In sum, Figure 2 evidences that the IRPs and the WGAN-GP synthesize the time series successfully.

For the next process, a Brownian Motion with $\mu = 0.05$ and $\sigma = 1$ shown in Figure 3, we also find the UMAP algorithm to create multiple heterogeneous clusters of real and synthetic elements. The long-drawn shape of the clusters allows for a more thorough inspection. Inside each cluster, the synthetic elements spread between the real data points, fill the missing space, and augment the green dots in a plausible manner.

Similar to the previous example, the generated IRPs and time series of Figure 3 do not show irregularities and appear realistic.

Testing our approach on real data requires a preprocessing step since WGAN-GP synthesizes IRPs evolving from a fixed value c . Real life time series have arbitrary start values. Therefore, the feature values could immediately reveal whether a time series sequence is real or synthetic. To remedy this, we rescale the original time series sequence to start from a fixed c . Without loss of generality, we set $c = 100$. For a last visual inspection, we use $N = 1681$ observations of the adjusted closing price of the Google stock and create rescaled sequences of length $d = 28$. The UMAP plot in Figure 4a) shows two large, drawn-out, heterogeneous clusters of real and synthetic elements. Similar to the previous experiments, the synthetic data is well spread across each cluster, which indicates a high sampling diversity. In case the sampling lacks diversity, there would be more synthetic data concentrated in isolated regions of the plot. The size of

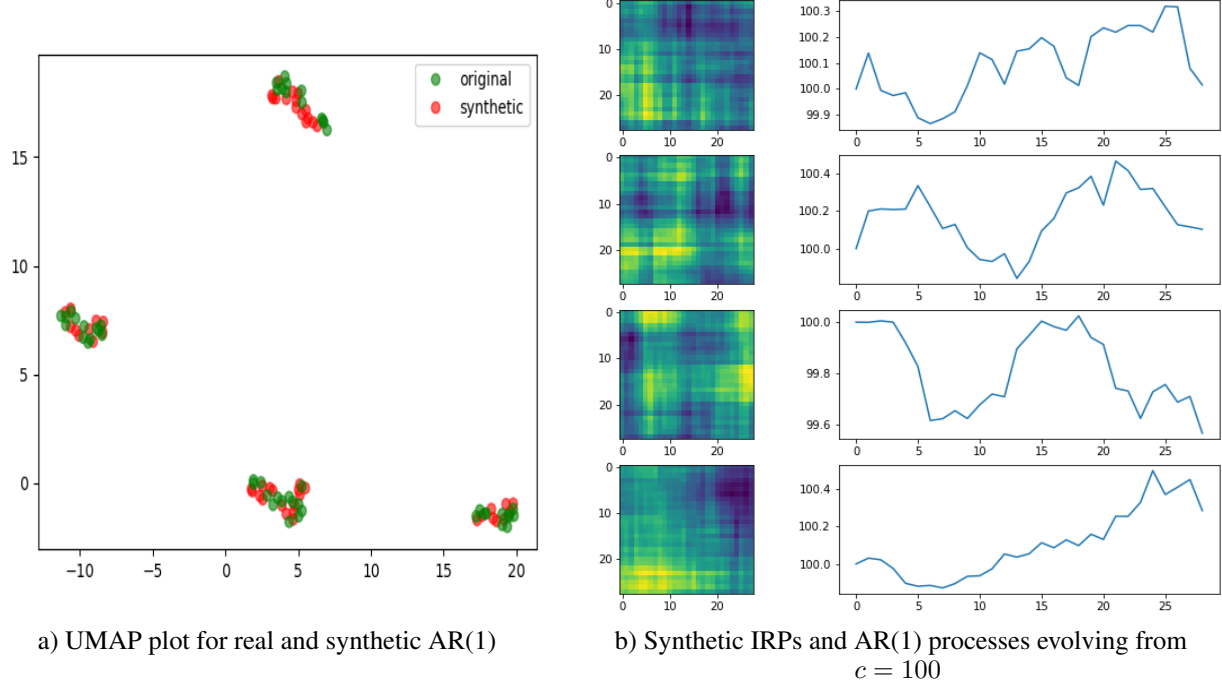


Figure 2: Simulation results for an AR(1) process

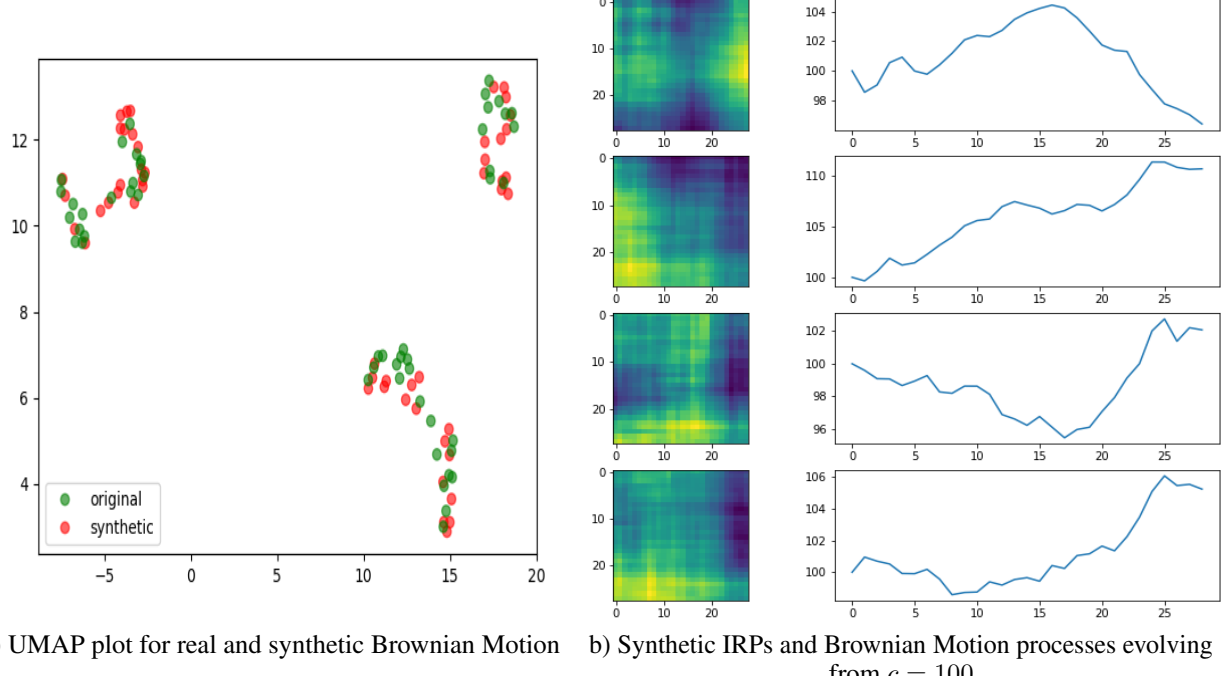


Figure 3: Simulation results for a Brownian Motion

the cluster indicates the increased complexity compared to the AR process. A look at Figure 4b) again supports the impression of the UMAP plot.

For the next set of experiments, we require quantifiable and comparable measures of model performance. Therefore, we benchmark the WGAN-GP with IRP representation against a state-of-the-art generative time series model. We choose TimeGAN as reference model since it outperformed various generative time series models such as RCGAN

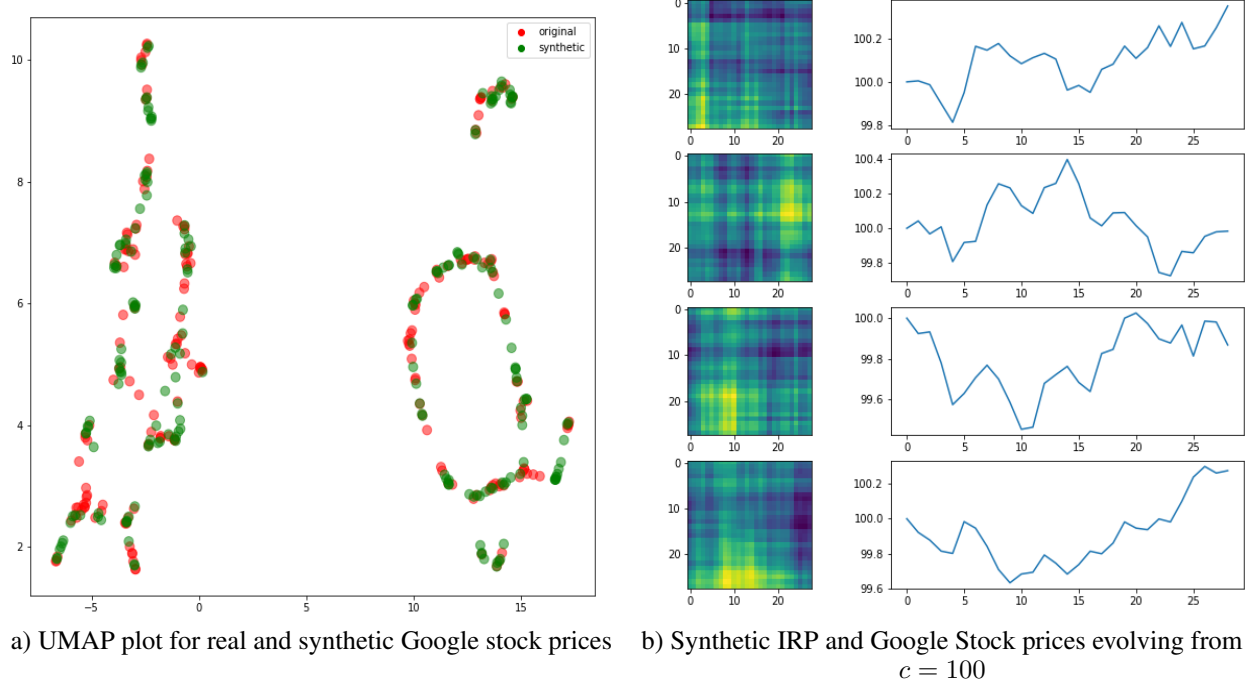


Figure 4: Simulation results for the adjusted close of Google stock price

(Esteban et al., 2017), WaveNet (Oord et al., 2016) and WaveGAN (Donahue et al., 2019). For our benchmark, we train TimeGAN for 10K epochs on the adjusted closing price of the Google stock introduced with the configuration from the Yoon et al. (2019) paper. The WGAN-GP uses the configuration of Gulrajani et al. (2017) with the only exception of a lower batch size of $b_{new} = 8$ compared to $b_{old} = 16$. We found a lower batch size to substantially improve the mean generator loss of WGAN-GP and its generalization ability during training.

We also conduct two backtests to support the results and evaluate different generative characteristics. The first backtest trains a model on synthetic data to predict real data. The rationale is that if the synthetic and original data are similar, a model trained on synthetic data should be able to predict original data. We train a gated recurrent unit (GRU) on synthetic data sequences from $t = 0$ up to $t = d - 1$ and predict the d^{th} element of each sequence. To obtain reliable results, we repeat the process $k = 10$ times and apply early stopping as a regularization technique before calculating the MAE on an original data test set. We then average the MAE over all k folds. The lower the MAE, the better the model synthesizes the data. The results of both TimeGAN and WGAN-GP with IRP can be found in Table 1.

In a second discriminative test, we use TimeGAN and WGAN-GP to generate synthetic data and let a GRU discriminate between original and synthetic data. In this test, lower (higher) classification accuracy indicates high (low) similarity between the synthetic and original data. Thus, the higher the binary classification error, the better the generated data. To avoid a classification by absolute values, we calculate returns since the synthetic data may exceed the maximum value of the initial data set, due to the arbitrary c used for sampling synthetic stock data. Again, we use early stopping and a test set for all $k = 10$ iterations before averaging the binary cross-entropy error. The results can be also be obtained from Table 1.

Regarding the predictive score, the WGAN-GP with IRP reduces the MAE by around 40% compared to the TimeGAN. This is a substantial increase in performance and demonstrates the potential of the IRP. Our approach also decreases the binary cross-entropy by roughly 45%, which is yet another major improvement in performance and indicates the quality of the generated data. However, we acknowledge that the standard deviation of the discriminative score is higher for WGAN-GP.

Throughout all experiments, hyperparameters such as batch size, epochs, and learning rates remained at the default value proposed in the TimeGAN paper or adjusted in a way that ensures convergence. Thus, we have a well-grounded statement on the competitive performance. Nonetheless, we cannot give all credit to the new representation since a comparison of two inherently different neural networks always leaves room for other factors that contributed to the success. Considering that the observed differences are substantial, we still conclude confidently that the proposed representation has substantially contributed to the improvement in performance. In appreciating this result, it is also

important to recall that the WGAN-GP model has a much simpler architecture with just one loss function and two networks compared to five loss functions and five networks in the TimeGAN model.

Model/Metric	Predictive Score on Prices (the lower the better)	Discriminative Score on Returns (the higher the better)
Yoon et al.	0.0125 +/- 9.8412e04	0.2715 +/- 0.09289796
WGAN-GP with IRP	0.0073 +/- 8.8183e04	0.4885 +/- 0.21295362

Table 1: Benchmarking Results

5 Conclusion

The paper introduced the concept of the IRP for image-based generative models. By design and backed by our experiments, we conclude that the IRP captures the underlying dynamics of time series well and fulfills the conditions of an invertible and scale-invariant representation, which facilitates recovering the time series. In the benchmark study, the IRP leverages the image-based generative model of a WGAN-GP to simulate realistic time series sequences, which outperform specialized RNN-based models, while simplifying the network structure and reducing the number of loss functions. The IRP facilitates benefiting from recent advances in computer vision and applying a manifold of advanced image-based generative models to time series data and for time series generation. A more thorough study on the statistical properties of the results and the generation of IRPs via alternative generative networks are a promising way to validate our results beyond this study. Other interesting paths to follow are the generation of IRPs from learned disentangled feature representations or extensions towards multivariate and conditional time series.

References

M. J. Afroni, D. Sutanto, and D. Stirling. Analysis of Nonstationary Power-Quality Waveforms Using Iterative Hilbert Huang Transform and SAX Algorithm. *IEEE Transactions on Power Delivery*, 28(4):2134–2144, October 2013. ISSN 0885-8977, 1937-4208. doi: 10.1109/TPWRD.2013.2264948. URL <http://ieeexplore.ieee.org/document/6616057/>.

Mohammed Ali, Mark W. Jones, Xianghua Xie, and Mark Williams. TimeCluster: dimension reduction applied to temporal data for visual analytics. *The Visual Computer*, 35(6):1013–1026, June 2019. ISSN 1432-2315. doi: 10.1007/s00371-019-01673-y. URL <https://doi.org/10.1007/s00371-019-01673-y>.

Martin Arjovsky, Soumith Chintala, and Léon Bottou. Wasserstein GAN. *arXiv:1701.07875 [cs, stat]*, December 2017. URL <http://arxiv.org/abs/1701.07875>. arXiv: 1701.07875.

Eoin Brophy, Zhengwei Wang, and Tomas E. Ward. Quick and Easy Time Series Generation with Established Image-based GANs. *arXiv:1902.05624 [cs, stat]*, October 2019. URL <http://arxiv.org/abs/1902.05624>. arXiv: 1902.05624.

David M. Curry. Practical application of chaos theory to systems engineering. *Procedia Computer Science*, 8:39–44, 2012. ISSN 18770509. doi: 10.1016/j.procs.2012.01.011. URL <https://linkinghub.elsevier.com/retrieve/pii/S1877050912000129>.

Chris Donahue, Julian McAuley, and Miller Puckette. Adversarial Audio Synthesis. *arXiv:1802.04208 [cs]*, February 2019. URL <http://arxiv.org/abs/1802.04208>. arXiv: 1802.04208.

J.-P Eckmann, S. Oliffson Kamphorst, and D Ruelle. Recurrence Plots of Dynamical Systems. *Europhysics Letters (EPL)*, 4(9):973–977, November 1987. ISSN 0295-5075, 1286-4854. doi: 10.1209/0295-5075/4/9/004. URL <https://iopscience.iop.org/article/10.1209/0295-5075/4/9/004>.

Cristóbal Esteban, Stephanie L. Hyland, and Gunnar Rätsch. Real-valued (Medical) Time Series Generation with Recurrent Conditional GANs. *arXiv:1706.02633 [cs, stat]*, December 2017. URL <http://arxiv.org/abs/1706.02633>. arXiv: 1706.02633.

Ian J. Goodfellow, Jean Pouget-Abadie, Mehdi Mirza, Bing Xu, David Warde-Farley, Sherjil Ozair, Aaron Courville, and Yoshua Bengio. Generative Adversarial Networks. *arXiv:1406.2661 [cs, stat]*, June 2014. URL <http://arxiv.org/abs/1406.2661>. arXiv: 1406.2661.

Ishaan Gulrajani, Faruk Ahmed, Martin Arjovsky, Vincent Dumoulin, and Aaron Courville. Improved Training of Wasserstein GANs. *arXiv:1704.00028 [cs, stat]*, December 2017. URL <http://arxiv.org/abs/1704.00028>. arXiv: 1704.00028.

Robert Hudson and Andros Gregoriou. Calculating and Comparing Security Returns is Harder than you Think: A Comparison between Logarithmic and Simple Returns. SSRN Scholarly Paper ID 1549328, Social Science Research Network, Rochester, NY, February 2010. URL <https://papers.ssrn.com/abstract=1549328>.

Phillip Isola, Jun-Yan Zhu, Tinghui Zhou, and Alexei A. Efros. Image-to-Image Translation with Conditional Adversarial Networks. *arXiv:1611.07004 [cs]*, November 2018. URL <http://arxiv.org/abs/1611.07004>. arXiv: 1611.07004.

Tero Karras, Samuli Laine, and Timo Aila. A Style-Based Generator Architecture for Generative Adversarial Networks. *arXiv:1812.04948 [cs, stat]*, March 2019. URL <http://arxiv.org/abs/1812.04948>. arXiv: 1812.04948.

Alireza Koochali, Peter Schichtel, Andreas Dengel, and Sheraz Ahmed. Probabilistic Forecasting of Sensory Data With Generative Adversarial Networks – ForGAN. *IEEE Access*, 7:63868–63880, 2019. ISSN 2169-3536. doi: 10.1109/ACCESS.2019.2915544. URL <https://ieeexplore.ieee.org/document/8717640/>.

N Marwan, M Carmenromano, M Thiel, and J Kurths. Recurrence plots for the analysis of complex systems. *Physics Reports*, 438(5-6):237–329, January 2007. ISSN 03701573. doi: 10.1016/j.physrep.2006.11.001. URL <https://linkinghub.elsevier.com/retrieve/pii/S0370157306004066>.

Leland McInnes, John Healy, and James Melville. UMAP: Uniform Manifold Approximation and Projection for Dimension Reduction. *arXiv:1802.03426 [cs, stat]*, September 2020. URL <http://arxiv.org/abs/1802.03426>. arXiv: 1802.03426.

Aaron van den Oord, Sander Dieleman, Heiga Zen, Karen Simonyan, Oriol Vinyals, Alex Graves, Nal Kalchbrenner, Andrew Senior, and Koray Kavukcuoglu. WaveNet: A Generative Model for Raw Audio. *arXiv:1609.03499 [cs]*, September 2016. URL <http://arxiv.org/abs/1609.03499>. arXiv: 1609.03499.

Hoo-Chang Shin, Neil A. Tenenholz, Jameson K. Rogers, Christopher G. Schwarz, Matthew L. Senjem, Jeffrey L. Gunter, Katherine Andriole, and Mark Michalski. Medical Image Synthesis for Data Augmentation and

Anonymization using Generative Adversarial Networks. *arXiv:1807.10225 [cs, stat]*, September 2018. URL <http://arxiv.org/abs/1807.10225>. arXiv: 1807.10225.

Warit Sirichotendumrong and Hitoshi Kiya. A GAN-Based Image Transformation Scheme for Privacy-Preserving Deep Neural Networks. *arXiv:2006.01342 [cs, eess]*, June 2020. URL <http://arxiv.org/abs/2006.01342>. arXiv: 2006.01342.

Kaleb E. Smith and Anthony O. Smith. A Spectral Enabled GAN for Time Series Data Generation. *arXiv:2103.01904 [cs, stat]*, March 2021. URL <http://arxiv.org/abs/2103.01904>. arXiv: 2103.01904.

Andrew Sutcliffe. Time-series forecasting using fractional differencing. *Journal of Forecasting*, 13(4):383–393, 1994. ISSN 1099-131X. doi: 10.1002/for.3980130404. URL <https://onlinelibrary.wiley.com/doi/abs/10.1002/for.3980130404>.

Paul Wilmott. *Paul Wilmott on quantitative finance*. Wiley, Chichester Weinheim, 2. editon, reprinted edition, 2006. ISBN 9780470018705.

L. Wyse. Audio Spectrogram Representations for Processing with Convolutional Neural Networks. *arXiv:1706.09559 [cs]*, June 2017. URL <http://arxiv.org/abs/1706.09559>. arXiv: 1706.09559.

Jinsung Yoon, Daniel Jarrett, and Mihaela van der Schaar. Time-series generative adversarial networks. In H. Wallach, H. Larochelle, A. Beygelzimer, F. d'Alché-Buc, E. Fox, and R. Garnett, editors, *Advances in Neural Information Processing Systems*, volume 32. Curran Associates, Inc., 2019. URL <https://proceedings.neurips.cc/paper/2019/file/c9e5f26cd17ba6216bbe2a7d26d490-Paper.pdf>.